Lidar observations of the middle atmospheric thermal tides and comparison with HRDI and GSWM. Part II: October observations at Mauna Loa (19.5°N).

Thierry Leblanc [1], I. Stuart McDermid [1], David A. Ortland [2]

[1] Jet Propulsion Laboratory
California Institute of Technology
Table Mountain Facility
Wrightwood, CA 92397

[2] Space Physics Research Laboratory
Department of Atmospheric, Oceanic and Space Sciences
University of Michigan
Ann Arbor, MI 48109-2143

To be Submitted to the Journal of Geophysical Research-Atmospheres, June 1998

Abstract

Using more than 145 hours of nighttime lidar measurements obtained during October 3-16, 1996 and October 2-11, 1997, the tidal signature in the middle atmospheric thermal structure (15-95 km) at Mauna Loa, Hawaii, (19.5°N) is investigated. The daytime HRDI temperatures taken in September and October 1993-1997 and zonally averaged at the same latitude are also used. The daytime HRDI and nighttime lidar temperature differences from their respective daytime and nighttime averages are compared to the equivalent differences predicted by the Global Scale Wave Model (GSWM) at the same latitude. Some consistent LST-related structures have been observed on both HRDI and lidar data suggesting the presence of important migrating tidal components. In particular, a warm period has been clearly identified, propagating downward from 105 km at 8:00 LST to 65 km at 00:00 LST and surrounded by two colder periods above and below. These warm/cold periods are predicted to occur two to three hours later by GSWM compared to the HRDI observations. Other LST-related structures have been observed by lidar between 30 and 80 km altitude, in particular a colder early night, warmer midnight, and colder late night around ~70 km suggesting a significant semidiurnal component at this altitude. As previously observed the amplitudes predicted by GSWM are much smaller than that observed by lidar and HRDI. The main point of disagreement between the lidar observations and GSWM predictions occurs between 60 and 85 km. A large semidiurnal component is observed by lidar leading to early and late cold night and warm midnight while no such large semidiurnal component is predicted by GSWM, leading to an apparent warm early night at 60 km, and an apparent cold midnight at 80 km and above. It appears that the tidal structure observed by lidar is more representative of that predicted by GSWM at 24°N, suggesting a latitudinal shift between theory and observation. It is not clear whether this shift is related to an indetermination of the tidal source and/or propagation or if the observed differences are simply due to local/regional Local-Solar-Time-related oscillations obscuring the tidal signature.

1. Introduction

The atmospheric response to the 24-hour periodic solar heating has been observed and studied for decades now. The very first observations recorded on a long-term basis included the diurnal (24-hours period) and semidiurnal (12-hours period) pressure variations on the ground. Then, using many instrumental techniques and using the classical tidal theory [*Chapman and Lindzen*, 1970; *Forbes*, 1982] it was found that even larger variations in pressure, density, temperature and wind occur in the middle atmosphere, especially above 80 km. Although the Fourier decomposition of the global atmospheric response to a 24-hour periodic forcing theoretically provides a 24-hour component plus all of its sub-harmonics (12-hour, 8-hour, etc.), the diurnal and semidiurnal components remain the dominant tidal periods in the entire middle atmosphere (10-110 km). A tutorial review on the atmospheric tides is provided, for example, by *Forbes* [1995]. The tidal winds in the Mesosphere-Lower-Thermosphere (MLT) region have been extensively studied at almost all latitudes. In particular, a strong diurnal signature in the zonal wind has been observed at the equator and in the meridional wind at tropical latitudes with a relatively well defined seasonal cycle [*Burrage et al.*, 1995; *Khattatov et al.*, 1997], and a dominant semidiurnal signature has been observed at mid- and higher-latitudes [*Manson et al.*, 1989; *McLandress et al.*, 1996]. On the other hand, very few observations of the thermal tides in the middle atmosphere and MLT region have been performed, mostly due to the lack of reliable instrumental techniques for measuring the neutral temperature above 60 km altitude. This lack of temperature measurements is even more critical at latitudes lower than 40° where ground-based instruments are particularly sparse. Therefore there is a crucial need for extensive studies on the thermal tides in the stratosphere and mesosphere, especially southward of 30°N, in order to quantify their importance and their role in the middle atmospheric dynamics as well as to better understand the MLT coupling.

This paper is the second part of a series of papers presenting results on the middle atmospheric thermal tides obtained from nighttime lidar measurements. The detailed description of the analysis and

methodology is presented in part I [*Leblanc et al.*, Submitted to JGR] together with some results obtained at Table Mountain (34.4°N) during the late winters of 1996/97 and 1997/98. This second part contains a description of the results obtained in October 1996 and 1997 at Mauna Loa Observatory (MLO, 19.5°N). The methodology follows exactly that described in part I and we strongly recommend the reader to refer to its sections 1 to 4. In this study, nighttime temperature profiles (15-95 km) obtained by the Jet Propulsion Laboratory (JPL) Rayleigh/Raman lidar located at MLO [*McDermid et al.*, 1995], and daytime winter temperature profiles (60-110 km) from the High Resolution Doppler Interferometer (HRDI) [*Ortland et al.*, 1998] onboard the Upper Atmosphere Research Satellite (UARS) have been used and compared to the October outputs of the Global Scale Wave Model (GSWM) [*Hagan et al.*, 1995]. The study focuses on the lidar results since the HRDI data set remains statistically limited. After a brief description of the instruments, methodology and data processing (section 2), the lidar nighttime and HRDI daytime evolution of the middle atmospheric temperature is compared to its GSWM equivalent (section 3). Then, using the method and arguments presented in part I [*Leblanc et al.*, Submitted to JGR], estimations of the phases and amplitudes of the diurnal and semidiurnal components are calculated and compared to those from the GSWM (section 4).

2. Instruments, data sets and data processing

a. Rayleigh and Raman-vibration Lidar temperatures:

Laser radiation transmitted into the atmosphere is backscattered by the molecules in the atmosphere and collected by a telescope. When the Mie scattering due to the aerosols particles is negligible compared to the molecular scattering (i.e. above 30 km), and assuming that the only non-negligible absorption in the atmosphere is due to ozone, the number of photons received is proportional to the number of photons emitted in the laser pulse and to the number of air molecules (or air density). When the Mie scattering is not negligible (basically below 30 km) and the Rayleigh method consequently turns inadequate, the atmospheric relative density can be determined using the Raman-vibration scattering of the nitrogen

molecule. This scattering is much less efficient than Rayleigh scattering but relatively insensitive to the presence of aerosols, making its use more appropriate at altitudes between 15 and 30 km. For both Rayleigh and Raman-vibration scattering methods, the temperature is deduced from the relative density using the hydrostatic equilibrium and ideal gas law assumptions. A priori temperature information is needed at the top of the profile and is usually taken from climatological models like CIRA-86. The total error in the temperature at the top due to this a priori initialization can be larger than 20 K but rapidly decreases as the temperature profile is integrated downward (typically divided by a factor of 3 every 10 km). Some description of the Rayleigh/Raman lidar and temperature retrieval techniques and a detailed review of the different sources of temperature uncertainty is given by for example by *Leblanc et al.* [1998a]. The lidar results described in this paper were obtained using the JPL Rayleigh/Raman lidar located at Mauna Loa Observatory (MLO, 19.5°N, 155.6°W). Due to its low-latitude location and due to the expected seasonal variations of the tides at these latitudes, we focused on the fall equinox. 8 nights from October 3-16, 1996, and 9 nights from October 2-10, 1997 were used, with a maximum of 10 hours of continuous measurements per night. A total of 145 hours of measurements were available, distributed from 19:00 to 5:00 LST.

b. HRDI temperatures:

HRDI measures brightnesses in the O_2 atmospheric A-band by observing the earth limb with line of sight tangent heights between 50 and 115 km. This brightness is basically proportional to both the band volume emission rate and an emission cross section which is a function of temperature and the emission line within the band. The profiles of brightness measurements from two consecutive limb scans (in which different lines within the A-band are measured) are inverted together to provide both a temperature and a band volume emission rate profile. For more details, see *Ortland et al.* [1998].

The space-time coverage of HRDI data depends on the UARS orbital period (96 min), the orbital inclination (57°) and the orbital precession rate (72 day). A tangent point track intersects a latitude circle

twice within its coverage range, once in the ascending node and once in the descending node. At the latitude of MLO only one of these nodes occurs during the day time (when HRDI can make temperature measurements). The closest pair of crossings will occur after 15 orbits (one day), and the second of these will be 6° longitude to the west of the first. At the latitude of MLO, this gives a separation of 630 km, with a 20 min local time delay, and eventually a HRDI overpass of MLO within 600 km once every ~4 days. Insufficient information was available from the geographical near-coincidences alone and to obtain a significant statistical basis, all longitudinally averaged HRDI temperature profiles taken in September and October between 1993-1997 at the latitude of MLO were used. A total of 72 profiles distributed over 8-hours between 8:00 and 16:00 LST were used for a comparison with the MLO lidar results. Due to the nature of the viewing modes, temperatures are recovered from 65 to 105 km, with the most accurate determination above 75 km.

3. Nighttime evolution of temperature: Comparison with daytime HRDI and GSWM.

As explained in part I [*Leblanc et al.*, Submitted to JGR] the first step consists in taking several nights (days) of lidar (HRDI) measurements, during a given season, and summing the raw data taken at given Local Solar Times (LST) to obtain mean temperature profiles at given LST. Thus, most of the long-period gravity wave disturbances detected by lidar, most of the variability due to the planetary waves detected by HRDI, and most of the lidar and HRDI instrumental noise, which are believed to be random from one night (day) to another, are substantially reduced if not removed. The hourly mean temperature profiles obtained by lidar during the periods of October 1996, October 1997, and both October 1996 and 1997 together are plotted in figure 1. The smoothed aspect of the temperature profiles illustrates the effect of the geophysical and instrumental noise reduction. The mean profiles are time-shifted by 10 K per hour. The profile on the right side of each plot is the resulting nightly average profile. The CIRA-86 profile is shown by the dashed-dotted line for reference. Although the temperature profiles look very similar below 70 km in October 1996 and 1997, they appear to be different above, especially at altitudes above 84 km, with a maximum difference 30-40 K, suggesting an important interannual variability at these altitudes.

For the two periods of October 1996 and October 1997 taken separately, and for both periods taken together, the nightly average profile (~10 hours) was subtracted from each of the hourly mean profiles. This calculation was also made for the daytime HRDI temperatures obtained at the latitude of MLO in September and October 1993-1997, using the daytime average (~8 hours) instead of the nighttime average. The temperature differences obtained by lidar every hour between 19:00 and 5:00 LST and by HRDI between 9:00 and 16:00 LST are contoured as a function of altitude and time in plate 1. Due to the limited statistics, the HRDI data cannot be displayed for each year separately and therefore any interannual tidal variability could introduce some differences between HRDI and lidar. These differences are expected to be small compared to the tidal amplitudes and to the residual noise contained in both HRDI and lidar data sets. It should also be noted that the daily-mean temperature and the nightly-mean temperature can be very different, especially in the presence of a strong diurnal and a weak semidiurnal components. Moreover, because of the ground-based character of the lidar instrument, all migrating, non-migrating and LST-dependent local/regional effects are expected to be seen by lidar while the zonally averaged HRDI measurements will presumably be representative of the migrating components only. Consequently, perfect consistency between the observed structures in HRDI temperature differences and in the lidar differences should not be expected unless a strong migrating tidal component is present (i.e. large amplitudes are involved). The equivalent differences from the daytime average and from the nighttime average were calculated using the diurnal and semidiurnal components predicted in October by the GSWM at 19.5°N. Since there is no model output at this latitude an interpolation between the model outputs at 18°N and 21°N was made. Although ~20°N is a nodal region for the diurnal component, it appears that a simple phase and amplitude interpolation was sufficient to obtain correct phases and amplitudes at 19.5°N. Indeed the diurnal node characterized by a fast latitudinal phase variation and near-zero amplitudes occurs just North of 21°N. The GSWM differences from the daytime and nighttime averages are plotted in plate 2(a) with the same disposition as in plate 1. To illustrate how dissimilar the daytime and nighttime averages can be, plate 2(b) shows the GSWM differences from the true 24-hour average for both nighttime and daytime periods. While there is continuity between the daytime and

nighttime panels in plate 2(b) at sunset, as expected but not very pronounced, there is no apparent continuity in plate 2(a), especially around 70-80 km altitude. Yet continuity is observed in plate 1 between the daytime HRDI data and the nighttime lidar data. A warm period is clearly propagating downward from 105 km at 8:00 LST (HRDI) to 70 km at 00:00 LST (lidar), especially well defined in October 1997 (previously observed at TMF in winter in *Leblanc et al.* [Submitted to JGR]. Although HRDI and GSWM seem to be in reasonably good agreement above 72 km (aside from a 2.5 hours phase shift), there is a strong disagreement between lidar and GSWM above 60 km. GSWM predicts a cold period at 80-85 km and 22:00-23:00 LST while the lidar observed a warm period at the same time. Also, GSWM predicts a near zero difference from the nightly mean temperature at 70-72 km and 23:00 LST while the lidar observed a clearly warm period. The nighttime temperature behavior observed here by lidar has also been observed by lidar over Haleakala, HI (21°N) during the ALOHA-93 campaign [*States and Gardner*, personal communication].The only point of agreement between GSWM and lidar is located around 50-55 km, with a warmer early night and a colder late night. There is also disagreement between HRDI and GSWM around 70-72 km with a warm period observed by HRDI at 12:00-13:00 LST while a continuous cooling trend during all day is predicted by GSWM.

4. Diurnal and semidiurnal components as calculated from lidar measurement.

The work described in part I, section 5 [*Leblanc et al.*, Submitted to JGR] for TMF in winter has similarly been performed for MLO for the two periods of October 1996 and 1997, taken separately and together. The lidar temperature differences have been fitted iteratively, using estimations of the tidal phases and amplitudes, to extract both diurnal and semidiurnal components. Some computer simulations of tidal extraction were performed beforehand to ensure that the iterative extraction of the 12- and 24-hour components was possible even when using only a ~10-hour long nighttime measurement window. No such work was attempted for the HRDI differences since the measurement window was only 8 hours. As a starting point, figure 2 shows the results of the 2-component fits applied to the GSWM differences from the 10-hour average plotted in plate 2(a) between 19:00 and 5:00 LST. The true GSWM diurnal and

semidiurnal amplitudes are plotted with solid lines with no error bars and the amplitudes calculated by the fits are plotted with solid lines with error bars. The true GSWM diurnal and semidiurnal phases are plotted with triangles and the phases calculated by the fits are plotted with circles with error bars. As expected, some regions of constant diurnal phase with height located near 18:00 and 6:00 LST alternate with some regions of undetermined phase located at 12:00 and 00:00 LST. The reasons for such alternating regions are explained in details in part I, section 4 [*Leblanc et al.*, Submitted to JGR]. Basically the regions of undetermined phase correspond to a true phase located at 12:00 or 00:00 LST while the regions of constant phase with height associated with a maximum amplitude and minimum standard deviations on amplitude and phase correspond to true phases located at 18:00 or 6:00 LST. Figure 3 is similar to figure 2 but the fit is now applied to the lidar data plotted in plate 1(c) (October 1996 and 1997 together). As already observed when comparing the nighttime evolution of temperature shown in plates 1 and 2(a), there are some important points of disagreement between the phases and amplitudes observed by lidar and predicted by GSWM above 55 km. Below 55 km the diurnal phase appears to be between 16:00 and 20:00 LST for both lidar and GSWM. The region of undetermined diurnal phase observed near 60 km in figure 3 would correspond to an actual phase near 12:00 LST. The diurnal phase predicted by GSWM at this altitude is around 17:00 LST. Also, a region of constant diurnal phase with height at 75-80 km associated with a maximum diurnal amplitude and a minimum standard deviation on the diurnal phase suggest a diurnal phase near 17:00-18:00 LST observed by lidar. At the same altitude, the diurnal phase predicted by GSWM is about 6:00 LST, which is nearly opposite to what is calculated from the lidar observations. Following the same method as that described by *Leblanc et al.*, [Submitted to JGR], an estimation of the correct diurnal phases and amplitudes can be made by comparing with the diurnal phases and amplitudes given by GSWM and using them as a "first guess". The observed diurnal phase seems to propagate downward from 17:00 LST at 76 km, to 5:00 LST at 63 km with an associated maximum in amplitude, then 6:00 LST at 59 km and again 18:00 LST at 55 km. It remains constant (~18:00 LST) down to 40 km, as predicted by GSWM. The estimated diurnal phases are in good agreement with the diurnal phases estimated from lidar measurements during ALOHA-93 [*Dao et*

al., 1995]. In particular, at 70-75 km both observations lead to estimated diurnal phases of 20:00-22:00 LST in total disagreement with the 8:00-9:00 LST predicted by GSWM between 18°N and 21°N. However the amplitudes estimated by Dao et al. [1995] are at least 30% larger than the amplitudes estimated here. The semidiurnal component calculated by the fit seems to be dominant (or at least of the same order as the diurnal) only at 44-, 59- and 70-km altitude. At these altitudes, the observed phases remain close to the semidiurnal phases calculated by GSWM. Plate 3 is similar to plate 2(a) but using the newly estimated components instead of GSWM. The agreement is good with both lidar and HRDI, suggesting that the estimates were correctly determined. To ensure this, a 24-hour averaged profile was estimated and used to re-apply the two-component fit to the lidar data. Using each of the ten, hourly composite profiles (from 19:00 to 5:00 LST) and our estimations of the diurnal and semidiurnal phase and amplitude, ten independent 24-hour averaged profiles were calculated. Then a singular 24-hour averaged profile was obtained by taking the average. If the estimated phases and amplitudes were correct, the newly estimated 24-hour average should be equal or close to each of the ten 24-hour independent averaged profiles and the results from the fit applied to the differences from this 24-hour average would converge to the "first guess" (and true) components. More details on the method of calculating the estimated 24-hour average are given in [*Leblanc et al.*, Submitted to JGR]. As shown in figure 4, the fits do converge to the estimated values, indicating that the estimated 24-hour averaged profile is nearly correct.

9. Discussion and conclusion.

The study of the HRDI daytime and lidar nighttime evolution of the middle atmospheric temperature and its comparison with that predicted by GSWM has led to these principal results:

1) Some consistent LST-related structures have been observed on both HRDI and lidar data suggesting the presence of important migrating tidal components. In particular, a warm period has been clearly

identified, propagating downward from 105 km at 8:00 LST to 65 km at 00:00 LST and surrounded by two colder periods above and below.

2) Other LST-related structures have been observed by lidar between 30 and 80 km altitude, consistent with some previous lidar observations at similar latitudes during the ALOHA-93 campaign, in particular a colder early night, warmer midnight, and colder late night around ~70 km suggesting a significant semidiurnal component at this altitude.

3) The comparison with the outputs of the GSWM tidal model has pointed out some similarities but also some disagreement: As previously observed the amplitudes predicted by GSWM are much smaller than that observed by lidar and HRDI. Also the warm downward propagating period described in point (1) is predicted to occur two to three hours later by GSWM compared to the HRDI observations.

4) The main point of disagreement between the lidar observations and GSWM predictions occurs between 60 and 85 km. A large semidiurnal component is observed by lidar leading to early and late cold night and warm midnight while no such large semidiurnal component is predicted by GSWM, leading to an apparent warm early night at 60 km, and an apparent cold midnight at 80 km and above.

5) A strong interannual variability has been observed by lidar above 80 km. The difference in the shape of the profiles in October 1996 and 1997 (figures 1(a) and 1(b)) are accompanied by differences in the determination of the tidal components. Such interannual variability has been previously observed in the tidal winds over Hawaii by *Fritts and Isler*, [1994].

A new version of GSWM has recently been developed [*Hagan*, personal communication]. This new version (GSWM98) incorporates a recent 5-year wind climatology of background winds. Also the Rayleigh friction in the mesosphere has been modified. When the HRDI and lidar observations are compared to the outputs of GSWM98, the disagreements mentioned in point (3) are substantially reduced above 80 km. The amplitudes predicted by GSWM98 are larger than those predicted by the older version.

Also, the phase delay between the warm period propagating downward observed by HRDI (between 105 and 85 km) and predicted by GSWM is mainly removed. However, the large differences between the lidar observations and the GSWM predictions between 60 and 80 km remain. There are several possible explanations for such differences.

One possible explanation is the presence of local/regional effects which may lead to disturbances with periods between 10 and 30 hours. Gravity waves with 12-h or/and 24-h periods may be generated in the convectively active tropical troposphere and propagate upward. A strong diurnal cycle has been observed in the development of tropospheric convection due to the local orography. In particular the Big Island of Hawaii where MLO is located is formed by two high (>4000 m) volcanoes, and the oceanic humidity is uplifted on their slopes by the dominant trade winds. After sunset, all the convective clouds (sometimes deep convection clouds) rapidly collapse, leading to clear skies after midnight. This 24-hour periodic pattern is very pronounced in October in Hawaii, and might lead to LST-dependent wind and temperature disturbances in the middle atmosphere which would consequently affect the migrating and non-migrating tides with a 24-hour repeatability. Recent studies of the non-migrating effects have already shown that non-migrating latent heat sources and solar IR absorption can modulate significantly the diurnal migrating tide [*Hagan et al.*, 1997], and that some significant longitudinal variability in the diurnal winds could be attributed to non-migrating tides [*Khattatov et al.*, 1996].

Another possible explanation is related to the latitudinal position of MLO. Plate 4 and figure 5 are similar to plate 2(a) and figure 3 respectively but using the phases and amplitudes predicted by GSWM at 24°N instead of 19.5°N. It is clear that the tidal components change significantly in only 4-5° latitude. The reason is that ~20° latitude is a nodal region for the diurnal component. At 24°N the diurnal phase is located around 18:00 LST at 75 km instead of 7:00 LST at 19.5°N. Also the semidiurnal amplitude is 50% larger especially at 80 km and above. The resulting temperature departures from the nighttime average is still not in perfect agreement with the observations but much more consistent. This could indicate that GSWM is latitudinally imprecise. Several mechanisms may account for this uncertainty. The latitudinal

structure of the tidal modes (Hough modes for temperature) is believed to be distorted by the background winds and highly variable, especially for the higher modes. A climatological or/and approximate picture of the background winds in the tropics (in particular a shift by a few degrees latitude) might lead to non-negligible departures from the observations taken during limited periods (like 10 days in 1996 and 10 days in 1997) and not necessarily supporting a "climatological theory". The recent release of GSWM98 including new background winds and a modified Rayleigh friction has revealed some significant differences from the 1995 version. The 50% increase of the amplitudes and the 2-3 hours phase shift primarily above 80 km have pointed out the high sensitivity of the tidal wave to the background winds. Also the tides dissipation and transience are far from being fully resolved and understood, and some small or moderate quantitative inaccuracies would easily lead to a substantial shift of a few degrees in the latitudinal structure of the migrating and non-migrating tides in the nodal regions. This shows the importance of increasing extensive lidar temperature measurements in the middle atmosphere in order to have a more "climatological" overview of the nighttime temperature evolution.

Some other effects like the diurnal variation of ozone and the gravity-wave-tides interaction are also candidates. *Nakamura et al.* [1997] have pointed out the high variability of the diurnal winds (with a ~19-days periodicity found in Hawaii) and suggested the dominant role of the tidal modulation by gravity wave and the gravity wave feedback on the observed tidal structure. Also, a recent study has shown that latent heat released in the troposphere is a non-negligible source of tidal oscillations [*Forbes et al.*, 1997]. Using a different parameterization of the cloud coverage (and consequent latent heating) than that usually used in GSWM, the authors have shown that latent heat release in the troposphere could account for 30% (5-8 K) of the total migrating thermal tides in the 80-150 km region.

More investigations based on both observation and modeling are needed to give a more detailed explanation of the differences observed between lidar and GSWM. The increased number of sophisticated mechanistic and General Circulation Models (GCM) together with the results from additional full-night lidar campaigns might give some elements of answer in the future and contribute to a better understanding

of the role of the thermal tides in the middle atmosphere dynamics. In particular another lidar campaign is planned at MLO in October 1998, as well as an inter-comparison between the tidal signature observed at MLO (19.5°N) and La Réunion Island (21.5°S).

Acknowledgements

The work described in this paper was carried out at the Jet Propulsion Laboratory, California Institute of Technology under an agreement with the National Aeronautics and Space Administration. We are extremely grateful to Maura Hagan (NCAR) for invaluable discussions regarding GSWM and mesospheric tides.

References.

Burrage, M. D., R. A. Vincent, H. G. Mayr, W. R. Skinner, N. F. Arnold and P. B. Hays, Long-term variability in the solar diurnal tide observed by HRDI and simulated by the GSWM, *Geophys. Res. Lett.*, *22*, 2641-2644, 1995.

Chapman, S., and R. S. Lindzen, *Atmospheric tides*, 201 pp., D. Reidel, Norwell, Mass., 1970.

Dao, P. D., R. Farley, X. Tao, and C. S. Gardner, Lidar observations of the temperature profile between 25 and 103 km: evidence of strong tidal perturbation, *Geophys. Res. Lett.*, *22*, 2825-2828, 1995.

Forbes, J. M., Atmospheric tides 1. Model description and results for the solar diurnal component, *J. Geophys. Res.*, *87*, 5222-5240, 1982.

Forbes, J. M., Tidal and planetary waves, *The upper mesosphere and lower thermosphere: A review of experiment and theory*, Geophysical Monograph 87, 67-87, 1995.

Forbes, J. M., M. E. Hagan, X. Zhang, and K. Hamilton, Upper atmosphere tidal oscillations due to latent heat release in the tropical troposphere, *Ann. Geophys.*, *15*, 1165-1175, 1997.

Fritts, D. C. and J. R. Isler, Mean motions and tidal and two-day structure and variability in the mesosphere and lower thermosphere over Hawaii, *J. Atmos. Sci.*, *51*, 2145-2164, 1994.

Hagan, M. E., J. M. Forbes and F. Vial, On modeling migrating solar tides, *Geophys. Res. Lett.*, *22*, 893-896, 1995.

Hagan, M. E., J. L. Chang, and S. K. Avery, Global-scale wave model estimates of nonmigrating tidal effects, *J. Geophys. Res.*, *102*, 16,439-16,452, 1997.

Khattatov, B. V., V. A. Yubin, M. Geller, P. B. Hays and R. A. Vincent, Diurnal migrating tide as seen by the high-resolution Doppler imager/UARS 1. Monthly mean global meridional winds, *J. Geophys. Res.*, *102*, 4405-4422, 1997.

Leblanc, T., I. S. McDermid, A. Hauchecorne, and P. Keckhut, Evaluation and optimization of lidar temperature analysis algorithms using simulated data, *J. Geophys. Res.*, *103*, 6177-6187, 1998a.

Leblanc, T., I. S. McDermid, and D. A. Ortland, Lidar observation of the middle atmospheric thermal tides. Comparison with HRDI and GSWM. Part I: Methodology and winter observations over Table Mountain (34.4°N)"., *J. Geophys. Res.*, **(this issue)**, 1998.

Manson, A. H., C. E. Meek, H. Teitelbaum, F. Vial, R. Schminder, D. Kuschner, M. J. Smith, G. J. Fraser, and R. R. Clark, Climatologies of semi-diurnal and diurnal tides in the middle atmosphere (70-110 km) at middle latitudes (40-55°), *J. Atmos. Terr. Phys.*, *51*, 579-593, 1989.

McDermid, I. S., T. D. Walsh, A. Deslis and M. L. White, Optical systems design for a stratospheric lidar system, *Appl. Opt.*, *34*, 6201-6210, 1995.

McLandress, C., G. G. Shepherd and B. H. Solheim, Satellite observations of thermospheric tides: Results from the Wind Imaging Interferometer on UARS, *J. Geophys. Res.*, *101*, 4093-4114, 1996.

Nakamura, T., D. C. Fritts, J. R. Isler, T. Tsuda, R. A. Vincent, and I. M. Reid, Short-period fluctuations of the diurnal tide observed with low latitude MF and meteor radars during CADRE: Evidence for gravity wave/tidal interactions, *J. Geophys. Res.*, *102*, 26,225-26,238, 1997.

Ortland, D. A., P.B. Hays, W.R. Skinner and J.-H. Yee, Remote sensing of mesospheric temperature and $O_2(^1\Sigma)$ band volume emission rates with the high-resolution Doppler imager, *J. Geophys. Res.*, *103*, 1821-1835, 1998.

Figure Captions.

Figure 1. Nighttime evolution of the mean profiles measured by lidar at Mauna Loa Observatory, HI (MLO) for the periods of October 3-16, 1996 (a), October 2-11, 1997 (b), and October 1996 and 1997 together (c). Each profile has been shifted by 10 K per hour starting at ~19:00 LST and ending at ~5:00 LST. The profiles on the right side are the resulting nightly mean profiles.

Figure 2. Diurnal and semidiurnal phases (circles with error bars) and amplitudes (solid lines with error bars) calculated by fitting 10 hourly-mean nighttime (from 19:00 to 5:00 LST) temperature profiles (departures from the 10-hour average) as calculated by GSWM at 19.5°N in October. The true GSWM components are plotted with triangles (phases) and solid lines with no error bars (amplitudes x 2).

Figure 3. Same as figure 2, but for the MLO lidar temperature differences of October 1996+1997 (see plate 1c)) instead of GSWM. The true GSWM 19.5°N-October phases are plotted with triangles and the amplitudes (x2) with solid lines.

Figure 4. Same as figure 3, but using the differences from our own estimated 24-hour average instead of the actual 10-hour nighttime average. The estimated amplitudes are plotted with solid lines and no error bars and the estimated phases with triangles.

Figure 5. Same as figure 3, but plotting GSWM at 24°N instead of 19.5°N.

Plate Captions

Plate 1. Hourly-mean lidar (HRDI) temperature differences from their nighttime (daytime) average. a) lidar measurements at MLO during October 3-16, 1996, b) October 2-11, 1997, and c) October 1996 and 1997 together. The mean lidar profiles of figure 1(a) to (c) have been used. For HRDI, all temperature profiles taken at the latitude of MLO in September and October 1993-1997 have been used.

Plate 2. a) Same as plate 1 but the temperature differences were calculated using the phases and the amplitudes (x2) of the diurnal and semidiurnal components predicted by GSWM at 19.5°N in October. b) Same as plate 2(a) but using the true 24-h average instead of the daytime and nighttime averages.

Plate 3. Same as plate 2(a) but using our own estimated diurnal and semidiurnal phases and amplitudes.

Plate 4. Same as plate 2(a), but using the phases and amplitudes predicted by GSWM at 24°N instead of 19.5°N.

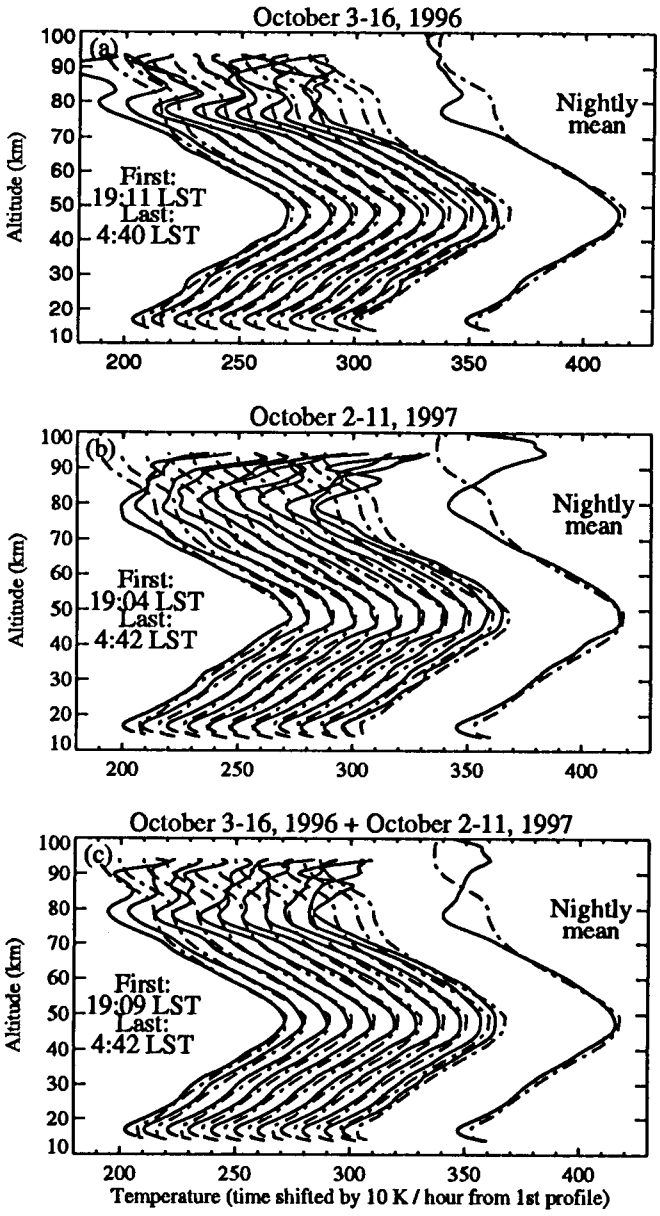
October 3-16, 1996
(a)
Nightly mean
First:
19:11 LST
Last:
4:40 LST
October 2-11, 1997
(b)
Nightly mean
First:
19:04 LST
Last:
4:42 LST
October 3-16, 1996 + October 2-11, 1997
(c)
Nightly mean
First:
19:09 LST
Last:
4:42 LST
Altitude (km)
Temperature (time shifted by 10 K / hour from 1st profile)

Figure 1

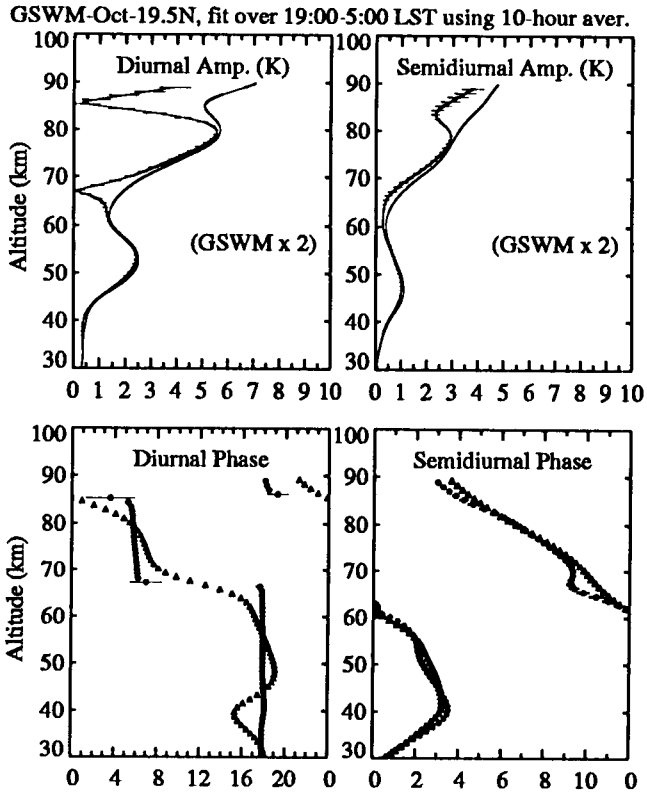
GSWM-Oct-19.5N, fit over 19:00-5:00 LST using 10-hour aver.
Diurnal Amp. (K)
(GSWM x 2)
Semidiurnal Amp. (K)
(GSWM x 2)
Diurnal Phase
Semidiurnal Phase
Altitude (km)
100
90
80
70
60
50
40
30
0 1 2 3 4 5 6 7 8 9 10
0 4 8 12 16 20 0
0 2 4 6 8 10 0

Figure 2

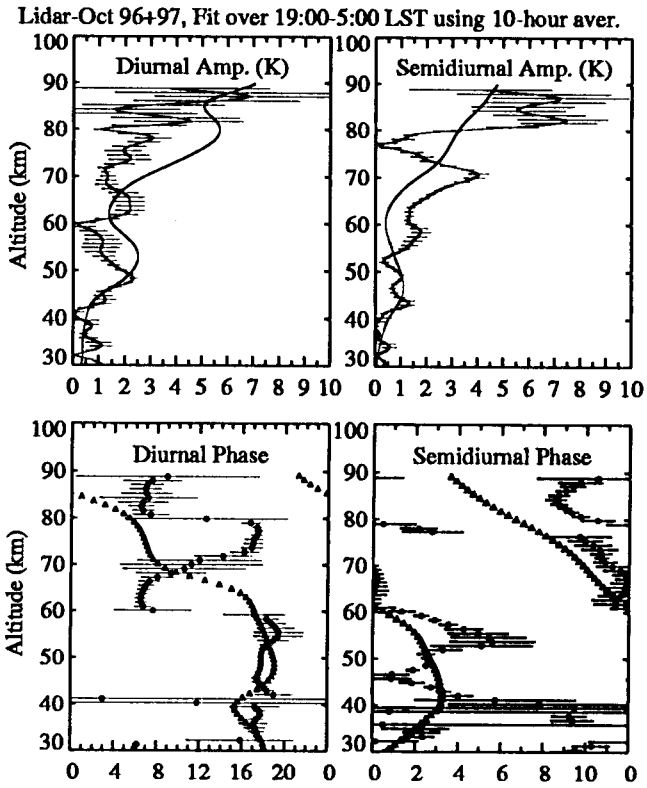
Lidar-Oct 96+97, Fit over 19:00-5:00 LST using 10-hour aver.
Diurnal Amp. (K)
Semidiurnal Amp. (K)
Diurnal Phase
Semidiurnal Phase
Altitude (km)
100
90
80
70
60
50
40
30
0 1 2 3 4 5 6 7 8 9 10
0 4 8 12 16 20 0
0 2 4 6 8 10 0

Figure 3

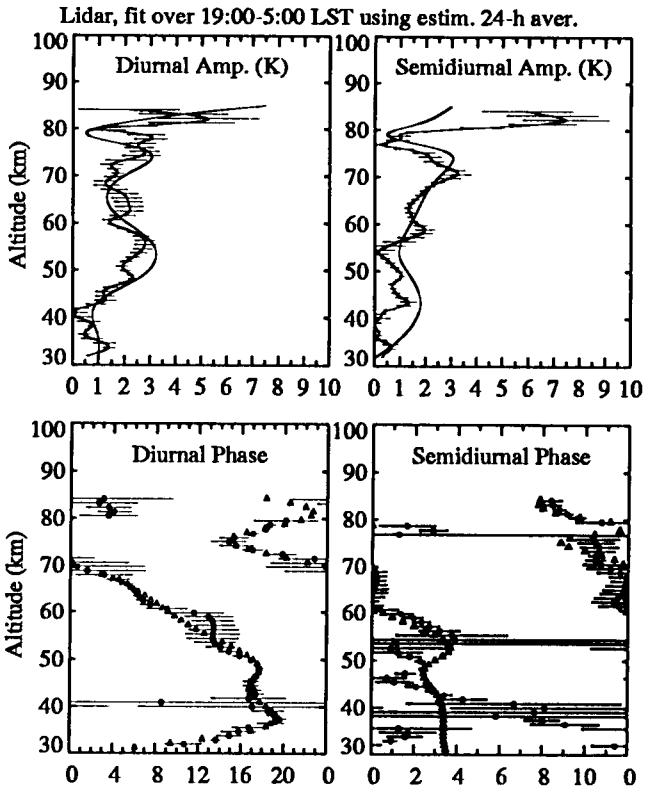
Lidar, fit over 19:00-5:00 LST using estim. 24-h aver.
Diurnal Amp. (K)
Semidiurnal Amp. (K)
Diurnal Phase
Semidiurnal Phase
Altitude (km)
Altitude (km)

Figure 4

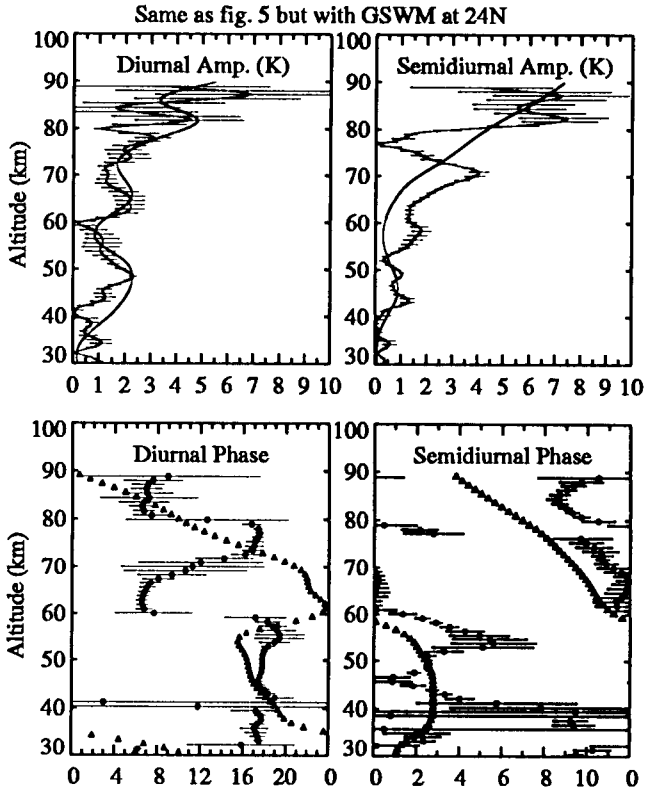
Same as fig. 5 but with GSWM at 24N
Diurnal Amp. (K)
Semidiurnal Amp. (K)
Diurnal Phase
Semidiurnal Phase
Altitude (km)
100
90
80
70
60
50
40
30
0 1 2 3 4 5 6 7 8 9 10
0 4 8 12 16 20 0
0 2 4 6 8 10 0

Figure 5

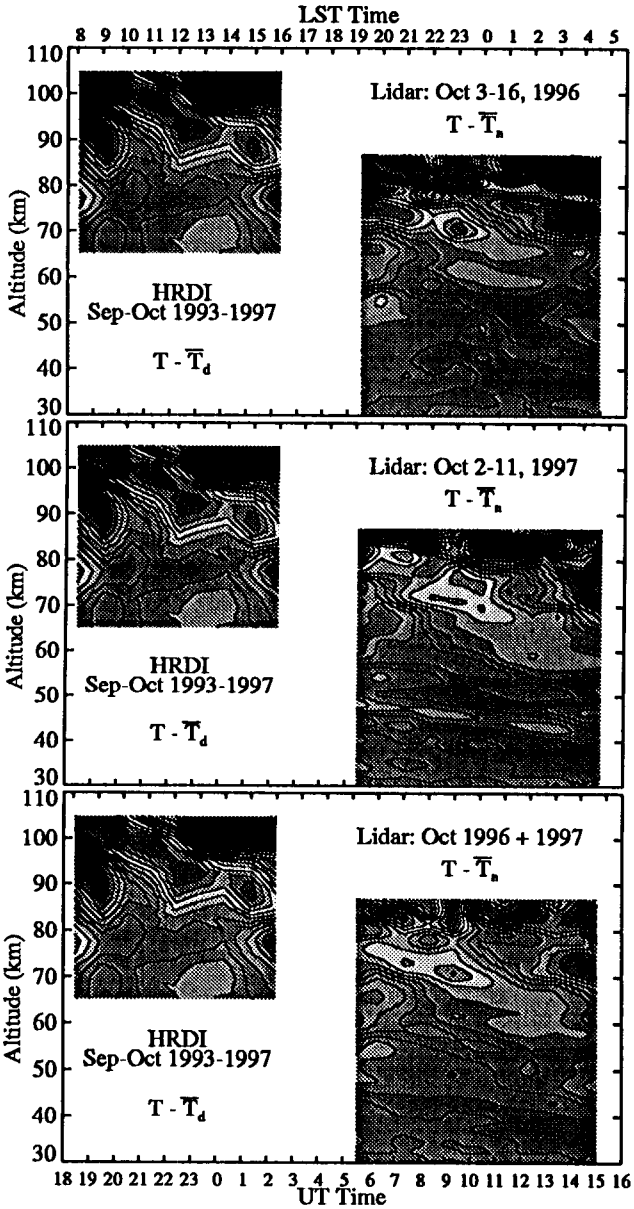

Plate 1

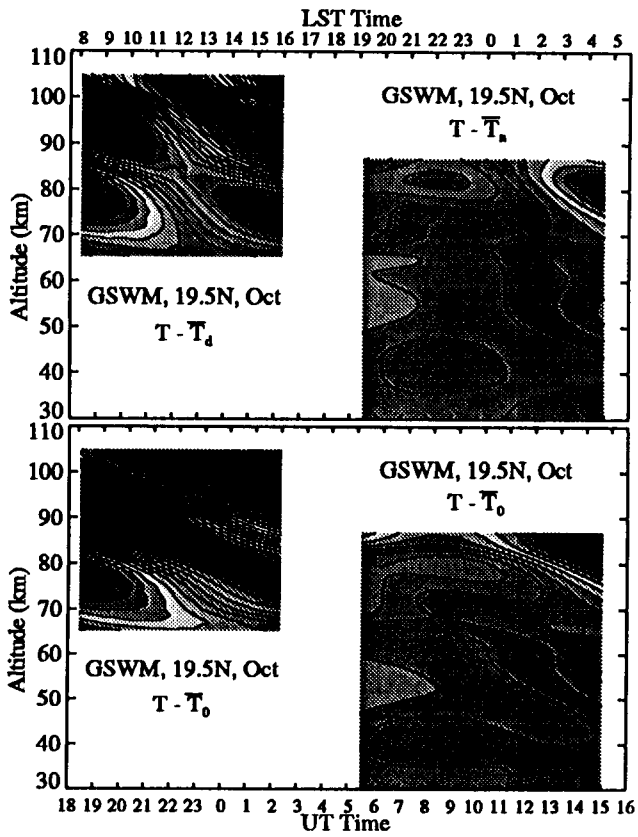

Plate 2

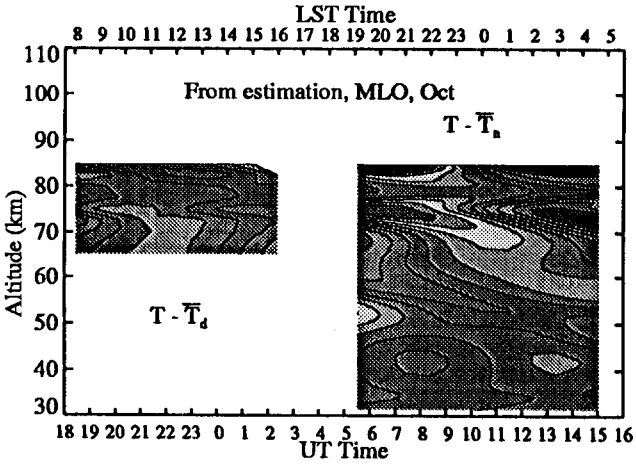

Plate 3

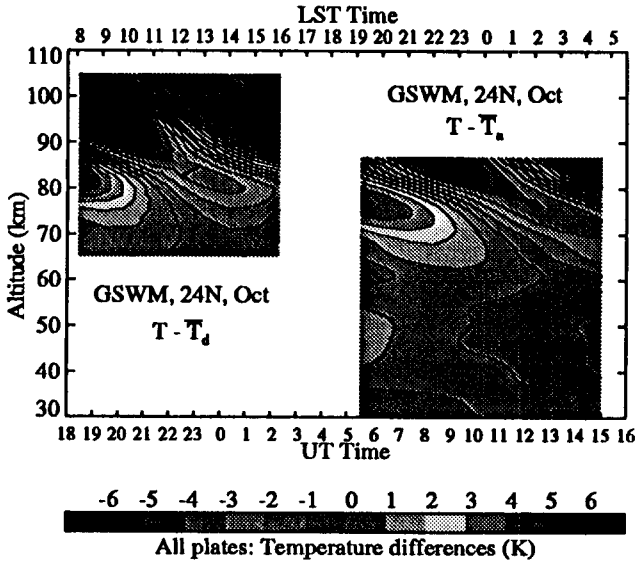

Plate 4